Applied Magnetic Resonance (2022) 53:949–961
https://doi.org/10.1007/s00723-021-01402-6

Applied
Magnetic Resonance

ORIGINAL PAPER

Mechanistic Study of Electron Spin Polarization Transfer in Covalent Donor–Acceptor-Radical Systems

Yuheng Huang[1] · Matthew D. Krzyaniak[1] · Ryan M. Young[1] · Michael R. Wasielewski[1]

Received: 30 April 2021 / Revised: 19 July 2021 / Accepted: 25 July 2021 /
Published online: 17 August 2021

Abstract

The mechanism of spin polarization transfer from a photogenerated spin-correlated radical pair to a stable radical was studied in a covalent donor-chromophore-acceptor-stable radical (D-C-A-R$^{\bullet}$) system, where the donor (D) is 4-methoxyaniline (MeOAn), the chromophore (C) is 4-(*N*-piperidinyl)-naphthalene-1,8-dicarboximide (ANI), the acceptor (A) is naphthalene-1,8:4,5-bis(dicarboximide) (NDI) and the stable radical (R$^{\bullet}$) is (2,2,6,6-tetramethylpiperidin-1-yl)oxyl (TEMPO). Experiments probed the effect of the spin–spin exchange interaction between D$^{\bullet+}$ and A$^{\bullet-}$ as well as the charge recombination dynamics of D$^{\bullet+}$-C-A$^{\bullet-}$ on spin polarization transfer from the D$^{\bullet+}$-C-A$^{\bullet-}$ SCRP to R$^{\bullet}$ as a function of the dielectric environment in glassy media at cryogenic temperatures. The results show that spin polarization on R$^{\bullet}$ is generated by asymmetry in the charge recombination pathways rather than variations in the spin–spin exchange interaction between D$^{\bullet+}$ and A$^{\bullet-}$. These results inform design criteria for using an SCRP to spin polarize a third spin for potential applications in quantum information science.

1 Introduction

The field of quantum information science (QIS) has attracted enormous interest and has developed into a highly interdisciplinary endeavor since Feynman's proposal for simulating physical systems using a quantum computer [1, 2]. The promise of the various potential applications of QIS, including quantum sensing, communication and computation, has motivated an extensive search for suitable quantum systems that fulfill the criteria for functional qubits [2–12].

✉ Michael R. Wasielewski
m-wasielewski@northwestern.edu

[1] Department of Chemistry, Center for Molecular Quantum Transduction, and Institute for Sustainability and Energy At Northwestern, Northwestern University, Evanston, IL 60208-3113, USA

Spin-correlated radical pairs (SCRPs) in organic donor–acceptor molecules can serve as spin qubit pairs (SQPs) and the relatively facile photogeneration of a well-defined initial SCRP quantum state offers a strategy to circumvent the typical spin initialization methods, which rely on thermal polarization at high magnetic fields and low temperatures (< 3 K) [10, 13, 14]. In the past, we have shown that SCRPs can be used to perform quantum teleportation and to implement a CNOT gate [15, 16].

The usefulness of SCRPs for QIS applications is generally not constrained by T_1 and T_2 relaxation times but by their intrinsic population lifetimes. One strategy to circumvent this lifetime issue and still exploit the well-defined initial state is to use the SCRP to polarize a third, persistent, electron spin with long relaxation times. While extensive work has been done on spin polarization transfer from a correlated SCRP to either an electron or nuclear spin in photosynthetic reaction centers [17–20], to the best of our knowledge no experimental study has varied both the magnitudes of the various spin–spin couplings and the kinetics of SCRP charge recombination in a fixed distance SCRP to ascertain how these factors influence polarization transfer from the SCRP to the third spin.

In the work presented here, we study the spin polarization transfer mechanism in covalent donor–acceptor-radical systems **1** and **2** (Scheme 1), where the donor (D) is 4-methoxyaniline (MeOAn), the chromophore (C) is 4-(*N*-piperidinyl)-naphthalene-1,8-dicarboximide (ANI), the acceptor (A) is naphthalene-1,8:4,5-bis(dicarboximide) (NDI) and the stable radical ($R^{\bullet}$) is (2,2,6,6-tetramethylpiperidin-1-yl)oxyl (TEMPO). Inclusion of a xylyl spacer in **2** leads to a smaller exchange interaction (J_{DA}) between $D^{\bullet+}$ and $A^{\bullet-}$ in the $D^{\bullet+}$-C-$A^{\bullet-}$ SCRP relative to that of **1** [21, 22]. Here, we show how the spin polarization of the stable nitroxide by the SCRP changes as a function of the SCRP recombination kinetics for two different values of J_{DA} between $D^{\bullet+}$ and $A^{\bullet-}$. Since the spin–spin exchange interactions between the radicals comprising the SCRP and $R^{\bullet}$ and the charge recombination (CR) pathways of the SCRP are key factors contributing to different spin polarization mechanisms [20, 23], assessment of the effects of these variables allows for identification of the mechanism that polarizes $R^{\bullet}$ in **1** and **2**.

1

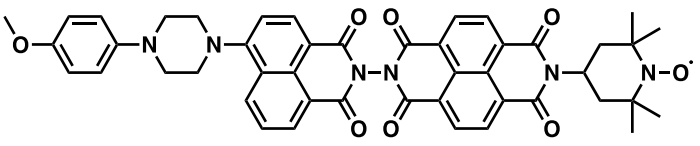

2

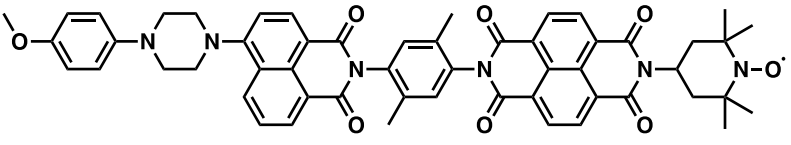

Scheme 1 Structures of 1 and 2

2 Theoretical background

Following photoexcitation, physical separation of the two entangled electron spins due to rapid charge transfer results in different hyperfine fields at the two spins. This, together with the difference in g-factors, has been shown to be the driving force for radical pair intersystem crossing (RP-ISC) in a magnetic field [24, 25], which results in the formation of an SCRP in a well-defined, spin-polarized, initial state even at high temperatures [13, 14, 26, 27]. This initial state can be probed using electron paramagnetic resonance (EPR) spectroscopy and the spin Hamiltonian for such a system in the rotating frame with microwave frequency ω_0 can be written in generic form:

$$\mathcal{H} = \sum_i (\omega_i - \omega_0) S_{iz} + \frac{1}{2} \sum_i \sum_{j \neq i} \left[a_{ij} S_{iz} S_{jz} + b_{ij} \left(S_{ix} S_{jx} + S_{iy} S_{jy} \right) \right] + \sum_i S_{iz} \sum_\alpha A_{i\alpha} I_{\alpha z} \tag{1}$$

where i and j are indices for the spins of interest, and α represents the nuclear spins responsible for the hyperfine fields [23, 25]. The first term in the Hamiltonian corresponds to the Zeeman interaction ($\omega_i = g_i \beta_e B_0 / \hbar$) with a static magnetic field B_0, the second accounts for spin–spin interactions between every pair of spins and the third covers hyperfine interactions. a_{ij} and b_{ij} are the secular and non-secular parts of the spin–spin interactions:

$$a_{ij} = -2J_{ij} + 2d_{ij}, b_{ij} = -2J_{ij} - d_{ij} \tag{2}$$

where J_{ij} is the exchange interaction and d_{ij} is the orientation-dependent dipolar coupling [20]. $A_{i\alpha}$ is the nuclear hyperfine coupling constant.

In an appropriate D-A system, photoexcitation initializes the SCRP into a $|S\rangle$ state However, $|S\rangle$ and $|T_0\rangle$ are not eigenstates of the two-spin Hamiltonian (Eq. 1), instead, the two eigenstates in such a system are mixtures of the $|S\rangle$ and $|T_0\rangle$ states. Due to this mixing, these levels are preferentially populated relative to the $|T_+\rangle$ and $|T_-\rangle$ states, resulting in a polarized two-spin system. The recombination dynamics are also influenced by this state mixing, depending on the character of the mixed state, wherein spin-selective recombination to either the singlet ground state or a local neutral triplet state is possible depending on the relative energies of the SCRP and the triplet state [28, 29]. At this point, spin evolution acquires additional degrees of freedom from variable reaction dynamics because the two recombination reactions act effectively as two separate reservoirs for depleted spin populations of the three-spin system. Thus, the exact recombination kinetics of a system directly determines the depletion of spin states, which in part controls the overall spin evolution.

The addition of a nuclear or electron spin to the two-spin SCRP system introduces new couplings as well as reaction pathways, resulting in various interesting effects that can be related to the initial coherent state mixing and preferential population of states in the two-spin system [18, 20, 21, 23, 28–33]. The most widely studied phenomena amongst these are photochemically induced dynamic nuclear polarization (photo-CIDNP) and electron polarization (photo-CIDEP), where the third spin (nuclear or electronic) acquires a non-Boltzmann population by interacting with the

initially entangled spin pair [18, 20, 23]. The interactions within the system can still be modelled using the generic Hamiltonian in Eq. 1 (note that for the 2-e-1-n case, one of the Zeeman terms comes from the nuclear spin), while the overall spin evolution of the density matrix can be described by the master Eq. [34, 35]:

$$\frac{\partial \rho}{\partial t} = -i[\mathcal{H}, \rho] - K_S\left[P_S, \rho\right]_+ - \sum_{n=-1,0,1} K_T\left[P_{T_n}, \rho\right]_+ \tag{3}$$

where $[A, B]_+$ denotes anticommutator $AB + BA$, and the projection operators P_k are used to address the spin-selective nature of the recombination process following the formalism used in Ref. [23]. K_S and K_T represent the spin selective recombination rates via the singlet and triplet pathways, respectively.

Numerical simulations based on Eq. 3 have been carried out previously to explain the polarization on the third spin in either the three-electron or the two-electron-one-nucleus case [20, 23]. Interestingly, for both phenomena, two different mechanisms can be derived from Eq. 3 although other factors may also contribute depending on the coupling regime within the systems. For a three-spin-mixing (TSM) mechanism to apply, anisotropic couplings between the third spin and each electron spin comprising the SCRP, as well as coupling within the SCRP, are needed to break the symmetry in populating the spin states of the third spin. In this scenario, the induced polarization is directly related to the polarization of the original SCRP and is sometimes referred to as polarization transfer [20]. This effect is only attributed to the anisotropic spin–spin interactions in spin evolution and therefore, should not depend on the reaction dynamics of the SCRP but solely the couplings across different individual spins.

Polarization in the differential decay (DD) mechanism, on the other hand, arises from the different singlet–triplet mixing efficiencies between the two stable radical sub-ensembles (α and β states of the third spin) [20, 23]. Although this mechanism also relies on an asymmetry within the SCRP seen by the third spin, it is ultimately the different decay rates in the spin-selective recombination reactions that result in the buildup of excess population in one spin state over the other in the third spin. In the photo-CIDNP literature, the different sub-ensembles in this mechanism are often presented as the cage and escape products in the chemical reactions for clarity [33]. In this case, the polarization of the additional spin is not only related to the asymmetric coupling of the SCRP with itself but also the recombination kinetics, whose effect was assessed by Salikhov et al. using the sign rule:

$$\Gamma = \left[\frac{\left(K_T - K_S\right)}{\left(K_T + K_S\right)}\right]\left(a_{DR^{\cdot}} - a_{AR^{\cdot}}\right)\left(\omega_D - \omega_A\right) \tag{4}$$

where a positive Γ suggests an emissive polarization pattern on the third spin and a negative Γ represents an absorptive one [20]. Some workers have even suggested that in this regime, the exchange interaction within the SCRP may not be needed for the third spin to be polarized [23].

Other mechanisms have also been proposed to explain photo-CIDNP and photo-CIDEP effects [35–38]. In our D-C-A-R$^{\bullet}$ system, for example, it is also conceivable

that polarization on the observer spin arises not from either of the two mechanisms discussed above, but simply from the interaction of the $R^{\bullet}$ spin with the two unpaired spins of the neutral triplet state of the CR product, which is known as the radical-triplet pair mechanism (RTPM). Ultimately, the number of interactions responsible for such a CIDEP effect could be manifold and depend on their relative magnitudes within the system, as well as reaction dynamics that can perturb the pure three-spin evolution. Understanding the exact mechanism responsible for the polarization of a third spin using SCRPs is important for designing molecular materials that can be useful for QIS applications [10]. Our experimental work is guided by the proposed mechanisms and aims to examine the effect of these key factors on the mechanism of photo-CIDEP.

3 Results and Discussion

To investigate the roles played by the TSM, DD and potentially other mechanisms in our D-C-A-$R^{\bullet}$ systems, we designed two sets of experiments to probe the effects of J_{DA} between $D^{\bullet+}$ and $A^{\bullet-}$ in the $D^{\bullet+}$-C-$A^{\bullet-}$ SCRP as well as the CR kinetics. Exchange coupling has been predicted to play an essential role in polarization transfer, while access to different recombination pathways influence polarization through the DD mechanism. The first experiment compares the nitroxide polarization magnitudes between **1** and **2**, where the donor and acceptor are identical and the difference in J_{DA} between them results from the additional xylyl spacer in **2** [22]. The second experiment investigates the polarization of **1** in different dielectric environments at cryogenic temperatures, which we have shown recently modulate the SCRP free energy (ΔG_{RP}) [30], and therefore determines whether CR occurs exclusively to the singlet ground state or can also occur to the lowest neutral triplet state of either D or A, which in **1** and **2** is D-C-^{3*}A. To minimize potential complications from spin diffusion and molecular motions, all experiments were done in cryogenic media, where intermolecular interactions should play little or no role in the polarization of $R^{\bullet}$.

To properly evaluate our spin polarization measurements, it is necessary to understand the electron transfer kinetics for the formation and decay of the SCRP of **1** and **2** at low temperature. Femtosecond and nanosecond transient absorption spectroscopy, fsTA and nsTA, respectively, were used to identify the intermediate species generated following photoexcitation and their appearance and decay rates (Figs. 1, S1, and S2). Global fitting of this data yields species-associated spectra (Figs. S1 and S2) along with the rate constants that are summarized in Table 1. Selective photoexcitation of C in **1** at 416 nm in butyronitrile (PrCN) at 105 K produces D-^{1*}C-A-$R^{\bullet}$ followed by initial formation of D-$C^{\bullet+}$-$A^{\bullet-}$-$R^{\bullet}$ in $\tau_{CS1} < 0.3$ ps as indicated by the formation of $NDI^{\bullet-}$within the instrument response, which has the distinct absorptions at 480 nm and 605 nm (Fig. 1a) [22, 27, 31]. The secondary charge transfer D-$C^{\bullet+}$-$A^{\bullet-}$-$R^{\bullet} \rightarrow$ $D^{\bullet+}$-C-$A^{\bullet-}$-$R^{\bullet}$ occurs in $\tau_{CS2} = 37 \pm 7$ ps. Inserting a xylyl spacer between C and A results in slower initial charge separation following photoexcitation of **2** in PrCN at 105 K, as well as a change in the order of the two-step electron transfer sequence, as evidenced by the observation of an initial strong absorption at 450 nm and the stimulated

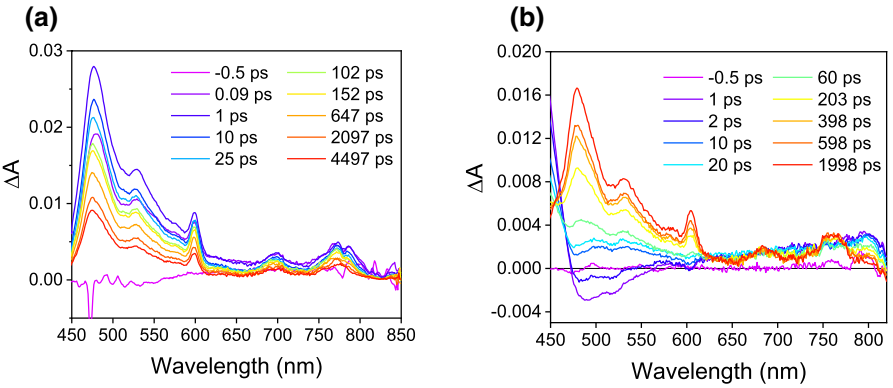

Fig. 1 Femtosecond transient absorption spectra of 1 **a** and 2 **b** in PrCN at 105 K. Both spectra were recorded following λex = 416 nm excitation

Table 1 Time constants of charge transfer steps for **1** and **2** under different conditions

	1 in PrCN at 105 K	**2** in PrCN at 105 K	**1** in toluene at 298 K	**2** in toluene at 298 K
τ_{CS1}(ps)	< 0.3	2.1 ± 0.2	< 0.5	7.0 ± 0.2
τ_{CS2}(ps)	37 ± 7	220 ± 3	< 1.0	400 ± 20
τ_{CR}	15.3 ± 0.3 ns 138 ± 4 ns[a]	4.33 ± 0.04 μs	49.9 ± 0.5 ns	506 ± 10 ns

[a] The additional time constant is a result of distributed kinetics due to the formation of different domains in the frozen solvent glass

emission band at 500 nm due to ^{1*}ANI (Fig. 1b) [22, 27, 31]. The disappearance of the stimulated emission and the emergence of a broad absorption band centered at 510 nm in τ_{CS1} = 2.1 ± 0.2 ps suggests that the first charge separation yields $D^{\bullet+}$-$C^{\bullet-}$-A-$R^{\bullet}$. The second charge transfer then takes place in τ_{CS2} = 220 ± 3 ps to produce $D^{\bullet+}$-C-$A^{\bullet-}$-$R^{\bullet}$, which again has absorptive features at 480 nm and 605 nm resulting from $NDI^{\bullet-}$. The charge recombination lifetimes of $D^{\bullet+}$-C-$A^{\bullet-}$-$R^{\bullet}$ were obtained by globally fitting the nsTA data (Figs. S3 and S4). The changes in charge separation rates at low temperature in PrCN exhibited distributed kinetics (Table 1) and can generally be rationalized using Marcus theory [39]. FsTA and nsTA spectra and kinetics for the corresponding molecules without $R^{\bullet}$, **3** and **4**, are given in Figs. S3 and S4 and Table S2 and are similar to those obtained for **1** and **2**.

While the charge separation process of **1** and **2** in PrCN at 105 K is similar to that in toluene at room temperature (Table 1), we did not observe the ^{3*}NDI state we reported earlier for the experiment done at room temperature in toluene [21, 22]. This is corroborated by the transient EPR experiments, which will be discussed in detail later. The energy levels of the different species can be estimated using the Weller formalism (Eqs. 5 and 6) to explain the different kinetics observed at low temperature [40], where Eq. 6 corrects for the solvation energy

differences between the low polarity glassy media and the polar solvents in which the redox potentials of D and A are measured.

$$\Delta G_{IP} = [E^{red}\left(D^{+}/D\right) - E^{red}(A/A^{-})] + \Delta G_{Sol} \tag{5}$$

$$\Delta G_{Sol} = -\frac{e^2}{4\pi\varepsilon_0}\left[\frac{1}{\varepsilon_s}\cdot\frac{1}{R_{DA}} + \left(\frac{1}{\varepsilon_{ref}} - \frac{1}{\varepsilon_s}\right)\left(\frac{1}{2r_{A^-}} + \frac{1}{2r_{D^+}}\right)\right] \tag{6}$$

In Eq. 6, ε_S and ε_{ref} refer to the dielectric constants of the solvents in which the charge transfers occur and in which the redox potentials are measured respectively, R_{DA} is the distance of the ion pair and r_{A^-} and r_{D^+} are the estimated ionic radii of D and A, assuming they can be approximated as spheres. The dielectric constant of the PrCN glass that forms at 105 K is slightly larger than that of toluene at room temperature [30]. Therefore, the solvent dielectric environment of glassy PrCN at 105 K shifts the energy level of the SCRP below the triplet energy level of ^{3*}A, effectively blocking the triplet recombination pathway (Fig. 2). While limitations in the transparency of glassy toluene limit extracting transient optical information using fsTA and nsTA, it is possible to obtain some information using time-resolved EPR (TREPR) spectroscopy, which will be discussed below. In contrast to **1** and **2** in PrCN, ^{3*}NDI was observed in both molecules in deuterated toluene at 85 K, while the decay time of the SCRP is similar to that in toluene at room temperature. This is consistent with the predictions of Eqs. 5 and 6 because the change in dielectric constant for toluene going from room temperature to 85 K is small.

Transient continuous wave and pulse EPR spectroscopies were used to study the evolution of the three-spin systems and to detect the polarization of the stable radical, respectively. Following photoexcitation of **2** in deuterated toluene, an intense spin-polarized TREPR signal (Fig. 3a) with an *e,a,e,a* pattern (where *a* = enhanced absorption, *e* = enhanced emission, low to the high field) was observed at X-band (~9.6 GHz), which was also observed in our previous

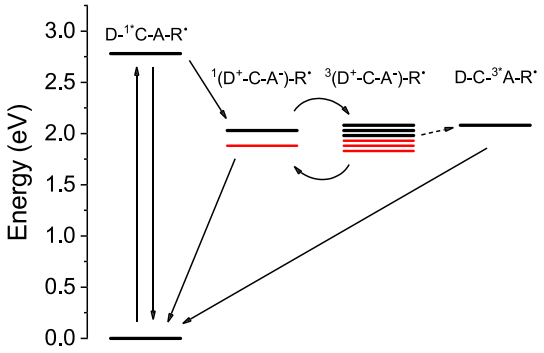

Fig. 2 Estimated energetics and relevant kinetic pathways for both 1 and 2 in different dielectric environments. The energy levels are not to scale. The black lines in the SCRP state represent the systems in nonpolar solvents such as toluene and the red lines represent those in more polar solvents such as PrCN. The dashed arrow to the 3*NDI state represents the triplet recombination pathway being "switched" on and off by modulated dielectric environments

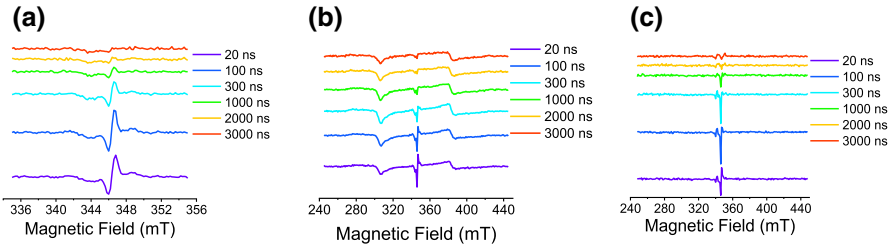

Fig. 3 TREPR spectra of **a** 2 in deuterated toluene with a 20 mT scan, **b** 2 in deuterated toluene with a 200 mT scan, and **c** 2 in PrCN with a 200 mT scan. The emissive signal at the center of (**c**) was interpreted as an artifact due to a wider field scan since a narrower scan only reveals the decay of an e,a,e,a pattern similar to (**a**). Simulations for the radical pair and triplet are available in the supplementary information

experiments at room temperature [31]. It has been shown that the *e*,*a*,*e*,*a* polarization pattern originates from a spin-polarized SCRP derived from a singlet excited state precursor with $J_{DA} > 0$ [17, 19, 24, 25]. The decay of this polarized SCRP signal is accompanied by the rise of a wider feature (Fig. 3b), which is attributed to the formation of ^{3}*NDI that results from SCRP recombination. A signal with an *e*,*a*,*e*,*a* pattern (similar to Fig. 3a) with a slightly different decay rate was detected for **2** in PrCN after photoexcitation. However, a wider magnetic field sweep did not reveal any broad features, suggesting the absence of ^{3}*NDI produced by CR of the SCRP within **2** in PrCN, confirming that at low temperature, CR pathways can be tuned by changing the dielectric environment of the SCRP.

A similar solvent effect was also observed in **1**, which was placed in three frozen glasses with different dielectric environments: PrCN, 9/1 v/v toluene/PrCN, and deuterated toluene. While the shorter-lived SCRP state of **1** compared to that of **2** was not observed, we were able to detect a ^{3*}NDI signal using TREPR in both 9/1 toluene/PrCN (Fig. 4b) and deuterated toluene (Fig. 4c). In different dielectric media, the triplet energy remains largely unchanged while the SCRP energy can be slightly shifted by the environment. Given that the SCRP and CR triplet in **1** and **2** are close in energy, a rough comparison of triplet yields across the three frozen media (Fig. 4) shows that lowering the SCRP energy by increasing the polarity of the medium slightly turns off recombination to the CR triplet. Note that there should be no net polarization of a neutral triplet state derived from recombination of a spin-correlated radical pair. The asymmetry observed in the spectra in Fig. 4 may be indicative of the influence of the TEMPO, but the exact mechanism remains to be determined.

Light-minus-dark (LMD) echo-detected field-swept experiments were used to compare the polarization magnitudes. We have observed anisotropy in the polarization of the different hyperfine transitions due to the nitrogen nuclear spin, which makes it difficult to quantitate polarization using the enhancement factor (f_E) common in the photo-CIDNP community [23]. Therefore, only qualitative differences in the LMD spectra relative to the dark spectra are treated as significant. Delay times between the excitation laser pulse and the first mw pulse have been selected based on reaction rates extracted from nsTA and TREPR data

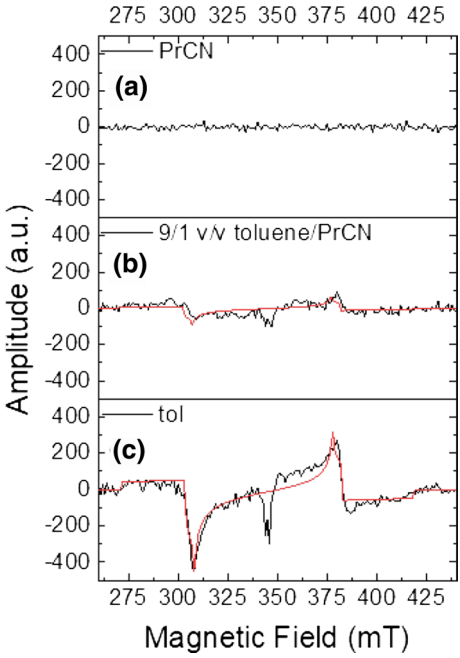

Fig. 4 Compound 1 in different solvents 2 μs after photoexcitation. Simulations of the wide triplet signal are shown in red. The decrease in signal amplitude as the fraction of PrCN increases is consistent with the prediction based on the Weller formalism

so that the mw pulses measure only the stable radical polarization after charge recombination of the SCRP.

In deuterated toluene at 85 K, we observed intense emissive polarization in both **1**, **2** (Fig. 5a and b), while the magnitudes of the polarization acquired by $R^{\bullet}$ for the two molecules relative to the $R^{\bullet}$ signal in the "dark" state were comparable. This suggests that the magnitude of J_{DA} is not the major factor in determining the polarization of the nitroxide radical. Results from the LMD experiments done on **1** in 9/1 v/v toluene/PrCN and PrCN, on the other hand, suggest that changing the SCRP recombination kinetics has a real effect on polarization on the third spin, e.g., in 9/1 toluene/PrCN the polarization greatly decreases (Fig. 5c), and in PrCN the light-minus-dark signal completely vanishes (not plotted). A similar trend was also

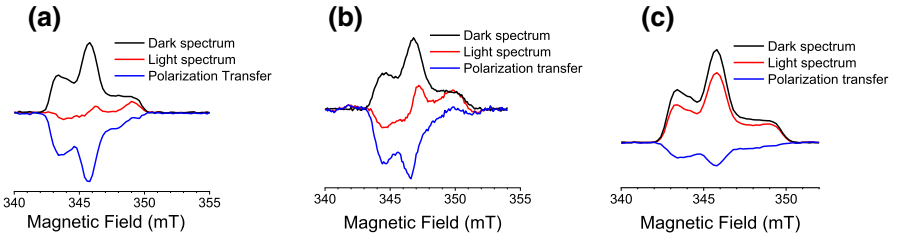

Fig. 5 Echo-detected field-swept light-minus-dark spectra of **a** 1 in deuterated toluene 1 μs after photoexcitation, **b** 2 in deuterated toluene 1 μs after photoexcitation, and **c** 1 in 9/1 v/v toluene/PrCN 1 μs after photoexcitation. The time delay corresponds to the interval between photoexcitation and the first π/2 pulse

observed in **2**. As the fraction of PrCN in the solvent increases, the dielectric environment becomes more polar, which lowers the SCRP state energy. The competition of singlet and triplet recombination pathways is largely dictated by the sign of the energy difference ΔE_{RP-T} between RP and the triplet state, [41] as suggested by the change in triplet yield according to the TREPR spectra (Fig. 4b). While the decrease in polarization can be directly correlated to the decrease in triplet yield, it is not yet clear whether polarization of the stable radical comes from the differential recombination kinetics or from coupling between the triplet state and the third electron spin.

To determine the source of the polarization, we carried out transient nutation experiments to study the multiplicity of TEMPO radical spin state following recombination of the SCRP in **2**, whose longer lifetime was more suitable for nutation studies. Nutation experiments were conducted with and without light in deuterated toluene at three different fields, which correspond to the three transitions due to nitrogen hyperfine splitting in the stable radical. The nutation signal was then Fourier transformed for identification of nutation frequency shift between the light and dark experiments. Representative light and dark nutation experimental data are plotted for the center hyperfine line (Fig. 6) and the lowest field hyperfine line of $R^{\bullet}$ (Fig. S7). For the source of polarization to be the triplet product of the charge transfer reactions, the stable radical would need strong coupling with the triplet, forming excited doublet and quartet states [36–38]. We have observed quartet state formation previously in several analogous arylenediimide triplet states coupled to stable radicals; [42, 43] however, the lack of direct evidence from the transient nutation experiment for quartet state formation in **1** and **2** makes it unlikely that the radical-triplet pair mechanism (RTPM) is the source of polarization on $R^{\bullet}$.

At this point, we have eliminated the three-spin-mixing (TSM) mechanism by comparing polarization magnitudes for molecules with the same building blocks but different values of J_{DA} between the donor and acceptor. It was shown that the formation of a local triplet state from charge recombination is necessary for the generation of polarized $R^{\bullet}$. Transient nutation experiments reveal that no quartet state forms

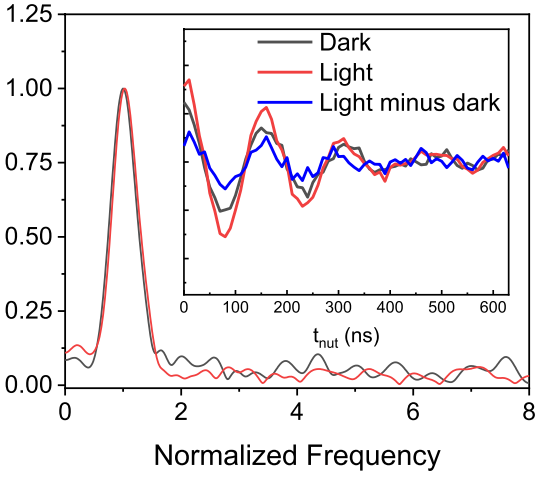

Fig. 6 Nutation frequency change at the center transition after photoexcitation. Inset: Integrated echo intensity as a function of nutation pulse (t_{nut}) length

following CR of the SCRP, ruling out the possibility that the direct coupling of $R^{\bullet}$ and ^{3*}NDI induces polarization on $R^{\bullet}$. In the meantime, the correlation between polarization magnitude and access to triplet recombination pathway, demonstrated using **1** in different dielectric environments, is supportive of the differential decay (DD) mechanism, where differential intersystem crossing efficiencies of the stable radical sub-ensembles α and β, caused by asymmetric coupling of $R^{\bullet}$ to $D^{\bullet+}$ and $A^{\bullet-}$, lead to the generation of "cage" and "escape" products with opposing signs on the population of $R^{\bullet}$, analogous to their nuclear spin counterparts in photo-CIDNP [20]. Finally, the different decay rates through singlet and triplet recombination pathways result in an excess of one of the "cage" and "escape" products, generating spin polarization on $R^{\bullet}$.

4 Conclusions

We demonstrated that the spin polarization transfer mechanism from an SCRP to a stable radical is analogous to the well-studied photo-CIDNP process. We have shown that differences in J_{DR} and J_{AR} are not sufficient to polarize $R^{\bullet}$. Careful design of the building blocks of the SCRP is needed to yield a suitable spin–spin interaction with greater anisotropy in its non-secular part for such an alternative means of polarizing the third spin to dominate. In contrast, controlling the charge recombination pathways using changes in the surrounding dielectric environment allows the system to be tuned to satisfy the specific requirements for using SCRPs in quantum information applications.

5 Further Information

This supplementary material includes structures for benchmark reference molecules, additional TA spectra and kinetics, TREPR spectra and simulation parameters.

Supplementary Information The online version contains supplementary material available at https://doi.org/10.1007/s00723-021-01402-6.

Acknowledgements This research was supported by the United States National Science Foundation under Award CHE-1900422.

Authors' contributions Not applicable.

Availability of data and material Contact corresponding author.

Code availability Not applicable.

Declarations

Conflicts of interest The authors declare no conflicts or competing interests.

References

1. A. Steane, Rep. Prog. Phys. **61**(2), 117–173 (1998)
2. T.D. Ladd, F. Jelezko, R. Laflamme, Y. Nakamura, C. Monroe, J.L. O'Brien, Nature **464** 45–53 (2010)
3. C.H. Bennett, D.P. DiVincenzo, Nature **404**(6775) 247–255 (2000)
4. L. Childress, M.V.G. Dutt, J.M. Taylor, A.S. Zibrov, F. Jelezko, J. Wrachtrup, P.R. Hemmer, M.D. Lukin, Science **314**(5797) 281–285 (2006)
5. M.H. Devoret, R.J. Schoelkopf, Science **339**(6124) 1169–1174 (2013)
6. L.M. Duan, M.D. Lukin, J.I. Cirac, P. Zoller, Nature **414**(6862), 413-418(2001)
7. N. Gisin, R. Thew, Nat. Photonics **1**(3), 165–171 (2007)
8. G. Kothe, M. Lukaschek, T. Yago, G. Link, K.L. Ivanov, T.-S. Lin, J. Phys. Chem. Lett. **12**(14), 3647–3654 (2021)
9. S. Schmitt, T. Gefen, F.M. Stuerner, T. Unden, G. Wolff, C. Mueller, J. Scheuer, B. Naydenov, M. Markham, S. Pezzagna, J. Meijer, I. Schwarz, M. Plenio, A. Retzker, L.P. McGuinness, F. Jelezko, Science **356**(6340), 832–837 (2017)
10. M.R. Wasielewski, M.D.E. Forbes, N.L. Frank, K. Kowalski, G.D. Scholes, J. Yuen-Zhou, M.A. Baldo, D.E. Freedman, R.H. Goldsmith, T. Goodson III, M.L. Kirk, J.K. McCusker, J.P. Ogilvie, D.A. Shultz, S. Stoll, K.B. Whaley, Nat. Rev. Chem. **4**(9) 490–504 (2020)
11. C.-J. Yu, M.D. Krzyaniak, M.S. Fataftah, M.R. Wasielewski, D.E. Freedman, Chem. Sci. **10**(6), 1702–1708 (2019)
12. C.-J. Yu, S. von Kugelgen, M.D. Krzyaniak, W. Ji, W.R. Dichtel, M.R. Wasielewski, D.E. Freedman, Chem. Mater. **32**(23), 10200–10206 (2020)
13. S. Nakazawa, S. Nishida, T. Ise, T. Yoshino, N. Mori, R.D. Rahimi, K. Sato, Y. Morita, K. Toyota, D. Shiomi, M. Kitagawa, H. Hara, P. Carl, P. Hoefer, T. Takui, Angew. Chem., Int. Ed. **51**(39) 9860–9864 (2012)
14. J.H. Olshansky, J. Zhang, M.D. Krzyaniak, E.R. Lorenzo, M.R. Wasielewski, J. Am. Chem. Soc. **142**(7), 3346–3350 (2020)
15. J.N. Nelson, J. Zhang, J. Zhou, B.K. Rugg, M.D. Krzyaniak, M.R. Wasielewski, J. Chem. Phys. **152**(1), 014503–014507 (2020)
16. B.K. Rugg, M.D. Krzyaniak, B.T. Phelan, M.A. Ratner, R.M. Young, M.R. Wasielewski, Nat. Chem. **11**(11), 981–986 (2019)
17. G.L. Closs, M.D.E. Forbes, J.R. Norris Jr., J. Phys. Chem. **91**(13), 3592–3599 (1987)
18. A.J. Hoff, P.J. Hore, Chem. Phys. Lett. **108**(1), 104–110 (1984)
19. P.J. Hore, D.A. Hunter, C.D. McKie, A.J. Hoff, Chem. Phys. Lett. **137**(6), 495–500 (1987)
20. K.M. Salikhov, A.J. Van der Est, D. Stehlik, Appl. Magn. Reson. **16**(1), 101–134 (1999)
21. E.A. Weiss, E.T. Chernick, M.R. Wasielewski, J. Am. Chem. Soc. **126**(8), 2326–2327 (2004)
22. E.A. Weiss, M.A. Ratner, M.R. Wasielewski, J. Phys. Chem. A **107**(19), 3639–3647 (2003)
23. G. Jeschke, J. Matysik, Chem. Phys. **294**(3), 239–255 (2003)
24. A.J. Hoff, P. Gast, S.A. Dzuba, C.R. Timmel, C.E. Fursman, P.J. Hore, Spectrochim. Acta, Part A **54A**(14), 2283–2293 (1998)
25. J. Tang, J.R. Norris, Chem. Phys. Lett. **233**(1-2), 192-200 (1995)
26. J.N. Nelson, M.D. Krzyaniak, N.E. Horwitz, B.K. Rugg, B.T. Phelan, M.R. Wasielewski, J. Phys. Chem. A **121**(11), 2241–2252 (2017)
27. S.R. Greenfield, W.A. Svec, D. Gosztola, M.R. Wasielewski, J. Am. Chem. Soc. **118**(28), 6767–6777 (1996)
28. J.A. Jones, K. Maeda, P.J. Hore, Chem. Phys. Lett. **507**(4–6), 269–273 (2011)
29. K. Maeda, P. Liddell, D. Gust, P.J. Hore, J. Chem. Phys. **139**(23) 234309 (2013)
30. H. Mao, R.M. Young, M.D. Krzyaniak, M.R. Wasielewski, J. Phys. Chem. Lett. **12**(9), 2213–2218 (2021)
31. Q. Mi, E.T. Chernick, D.W. McCamant, E.A. Weiss, M.A. Ratner, M.R. Wasielewski, J. Phys. Chem. A **110**(23), 7323–7333 (2006)
32. M.T. Colvin, R. Carmieli, T. Miura, S. Richert, D.M. Gardner, A.L. Smeigh, S.M. Dyar, S.M. Conron, M.A. Ratner, M.R. Wasielewski, J. Phys. Chem. A **117**(25), 5314–5325 (2013)
33. J.R. Woodward, Prog. React. Kinet. Mech. **27**(3), 165–207 (2002)
34. R. Haberkorn, Mol Phys **32**(5), 1491–1493 (1976)
35. T.P. Fay, L.P. Lindoy, D.E. Manolopoulos, J Chem Phys **149**(6) 064107 (2018)

36. C. Blaettler, F. Jent, H. Paul, Chem. Phys. Lett. **166**(4), 375–380 (1990)
37. Y.E. Kandrashkin, A. van der Est, Chem. Phys. **151**(18), 184301 (2019)
38. Y. Kobori, M. Fuki, H. Murai, J. Phys. Chem. B **114**(45), 14621–14630 (2010)
39. R.A. Marcus, J. Chem. Phys. **43**(2), 679–701 (1965)
40. A. Weller, Z. Phys. Chem. **133**(1) 93–98 (1982)
41. Y. Kobori, S. Sekiguchi, K. Akiyama, S. Tero-Kubota, J. Phys. Chem. A **103**, 5416–5424 (1999)
42. E.M. Giacobbe, Q. Mi, M.T. Colvin, B. Cohen, C. Ramanan, A.M. Scott, S. Yeganeh, T.J. Marks, M.A. Ratner, M.R. Wasielewski, J. Am. Chem. Soc. **131**(10), 3700–3712 (2009)
43. M. Mayländer, S. Chen, E.R. Lorenzo, M.R. Wasielewski, S. Richert, J. Am. Chem. Soc. **143**, 7050–7058 (2021)